ACS APPLIED MATERIALS & INTERFACES

Research Article

www.acsami.org

Porous Spherical Carbon/Sulfur Nanocomposites by Aerosol-Assisted Synthesis: The Effect of Pore Structure and Morphology on Their Electrochemical Performance As Lithium/Sulfur Battery Cathodes

Hiesang Sohn,[†] Mikhail L. Gordin,[†] Terrence Xu,[†] Shuru Chen,[†] Dongping Lv,[†] Jiangxuan Song,[†] Ayyakkannu Manivannan,[‡] and Donghai Wang*[,†]

[†]The Pennsylvania State University, Department of Mechanical and Nuclear Engineering, University Park, Pennsylvania 16802, United States

[‡]The Department of Energy-National Energy Technology Laboratory (DOE)/NETL Materials Performance Division, 3610 Collins Ferry Rd. P.O. Box 880, Morgantown, West Virginia 26507-0880, United States

Supporting Information

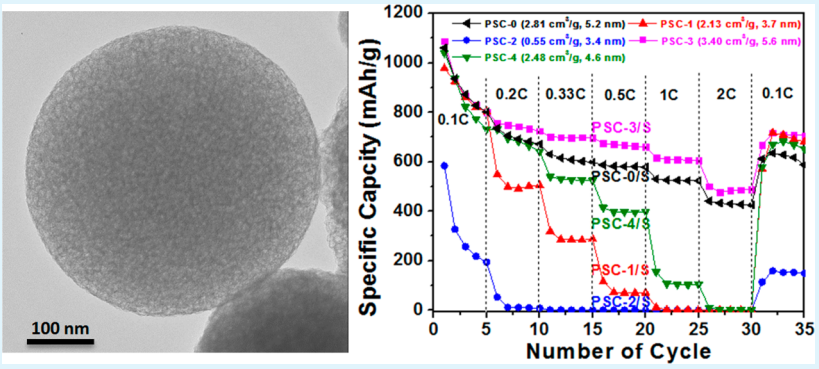

ABSTRACT: Porous spherical carbons (PSCs) with tunable pore structure (pore volume, pore size, and surface area) were prepared by an aerosol-assisted process. PSC/sulfur composites (PSC/S, S: ca.59 wt %) were then made and characterized as cathodes in lithium/sulfur batteries. The relationships between the electrochemical performance of PSC/S composites and their pore structure and particle morphology were systematically investigated. PSC/S composite cathodes with large pore volume (>2.81 cm^3/g) and pore size (>5.10 nm) were found to exhibit superior electrochemical performance, likely due to better mass transport in the cathode. In addition, compared with irregularly shaped carbon/sulfur composite, the spherical shaped PSC/S composite showed better performance due to better electrical contact among the particles.

KEYWORDS: *lithium/sulfur battery, aerosol-assisted process, porous spherical carbon, porosity*

1. INTRODUCTION

The increasing demand for high energy/power density energy storage for use in renewable energy applications has prompted keen interest in new electrode materials for rechargeable lithium ion batteries.[1−7] Lithium/sulfur (Li/S) batteries are considered to be a promising energy-storage technology owing to the high theoretical capacity (1672 mAh/g) and achievable specific energy (2600 Wh/kg) of sulfur.[4−9] Additionally, sulfur is low-cost, abundantly available, and eco-friendly, making Li/S batteries even more attractive.[4−7] However, the practical utilization of sulfur cathodes is limited due to their low columbic efficiency, low specific capacity, and fast capacity fading. These issues mainly originate from the dissolution, shuttling, and side reaction of lithium polysulfides (Li_2S_x, $2 < x \leq 8$),[9−11] the poor electronic and ionic conductivity of sulfur and Li_2S,[4−9,12,13] and the large volumetric expansion during lithiation of sulfur to Li_2S (80%).[13]

Many researchers have tried to address these issues by the development of new cathode materials.[4−7] Various cathode materials have been explored, mostly by forming a composite of sulfur and carbon[4,7,14,15] to increase conductivity of the cathode and confine lithium polysulfides.[4−7,13−15] Particularly, porous carbon/sulfur composite based electrodes using micro-[15,17,18] and mesoporous carbon[15,16,19−23] have been widely studied, as these materials are considered to have multiple benefits. First, the porous structure encapsulates sulfur, improving electrical contact and thus the conductivity of the cathode.[4,5,7,13−15]

Received: February 13, 2014
Accepted: April 23, 2014
Published: April 23, 2014

Scheme 1. Schematic of the Formation Process of Porous Spherical Carbon (PSC) Prepared through an Aerosol-Assisted Process[a]

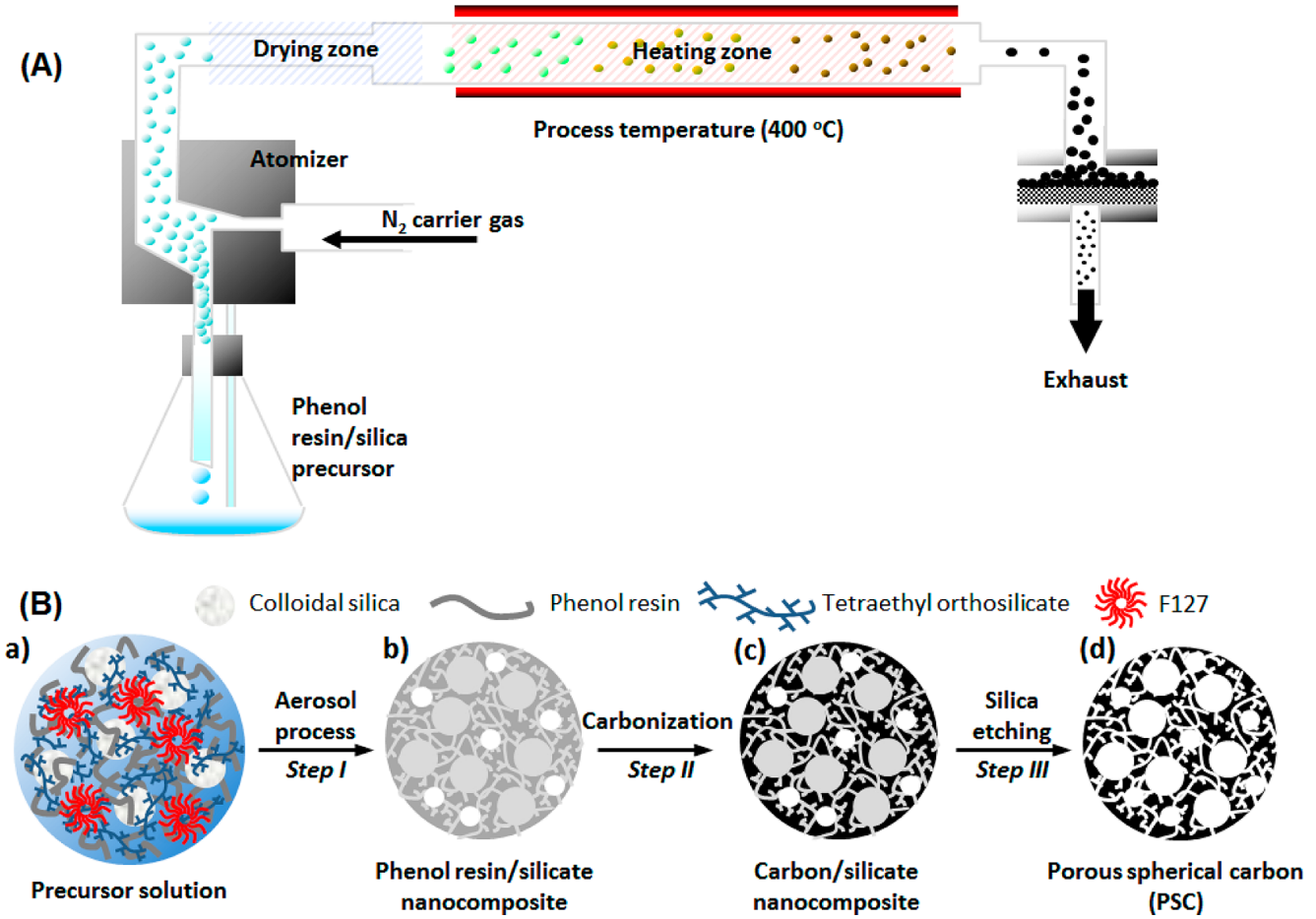

[a](A) Schematic of aerosol apparatus. (B) Formation process of porous spherical carbon: (a) precursor, (b) aerosol product, (c) carbonization product, and (d) final PSC product.

Second, the porous carbon can restrain the diffusion of dissolved polysulfides out of the cathode, thereby improving specific capacity and cycling stability.[4,5,15,23] Finally, the carbon framework also provides electron-conducting paths through the cathode, further improving conductivity and enabling faster lithiation/delithiation and improved sulfur utilization.[4−7,14,23] It is also important to tune the characteristics of the carbon hosts, such as the particle size, particle morphology, porosity, and surface area, since such characteristics can affect electrochemical performance.[24] Particularly, spherical carbon/sulfur composites with high packing density have been developed to improve the volumetric energy density of the sulfur cathode.[18,20,22,23] For example, Schuster et al. reported a porous nanosized spherical carbon/sulfur nanocomposite as a cathode for Li/S batteries.[20] Bimodal structured porous spherical carbon/sulfur composites were synthesized by a two-step casting process using colloidal silica from an inverse opal template, structure directing agent, and carbon precursor; these composites demonstrated good cycle stability and high capacity.[20] Zhang et al.[21] and Jayaprakash et al.[22] reported core/shell and hollow spherical carbon/sulfur composites and studied structure-enabled sulfur encapsulation and polysulfide migration inhibition to enhance electrochemical performance. The hollow structures were prepared by using SnO_2 hollow spheres[21] or spherical silica as the hard templates[22] for coating with carbon precursor, and corresponding sulfur composites were prepared, showing good cyclability[21,22] and high capacity[22] due to their unique structure. Recently, we presented a microsized spherical composite of mesoporous carbon, carbon nanotubes, and sulfur as a Li/S battery cathode, which was prepared by a combination of evaporation induced self-assembly and emulsion polymerization.[23] The synthesized porous spherical carbon supports a high sulfur loading (5 mg-S/cm^2) with high tap density (~1 g/mL) and shows good electrochemical performance.[23] While considerable efforts were devoted to developing novel spherical carbon/sulfur composite-based cathodes,[17−22] there have not been any systematic studies regarding the effect of the pore structure and particle morphology of spherical carbon on the electrochemical performance of the spherical carbon/sulfur composites.

Here, we present a facile and scalable synthesis of porous spherical carbon (PSC) with tunable pore structure (pore volume, pore size, and surface area) through a continuous aerosol-assisted process for use as a sulfur host in Li/S battery cathodes. The effects of pore structure on the electrochemical performance of PSC/sulfur (PSC/S) composite cathodes have been systematically investigated. PSC/S cathodes using PSC with large pore volume and pore size were found to exhibit enhanced electrochemical performance, while high surface area does not significantly affect the performance. Additionally, the

PSC/S composites exhibit superior performance to that of irregularly shaped carbon/sulfur composite with similar porosity, suggesting that the particle morphology of electrode materials is also important. These results can serve as guidance for design and fabrication of novel porous carbon/sulfur composite cathodes for high performance Li/S batteries.

2. EXPERIMENTAL SECTION

(1). Synthesis of the Porous Spherical Carbon/Sulfur (PSC/S) Nanocomposites. Spherical carbon/silica composite particles were first synthesized by an aerosol-assisted evaporation induced self-assembly (EISA) method[25,26] using a solution of phenol resin, tetraethyl orthosilicate (TEOS), colloidal silica, and surfactant as the precursor. Then, porous spherical carbon was generated by carbonization of the resin, burn-out of the surfactant, and etching away silica with hydrofluoric acid (HF) and was controlled by changing the precursor composition. Sulfur was loaded to porous spherical carbon by a melt-diffusion and evaporation under argon atmosphere.

Precursor Solution. Modified precursor for the synthesis of reported mesoporous carbon was used for the preparation of porous spherical carbon.[27] In a typical synthesis, 40 g ethanol, 1 mL 1 M HCl, and 8.25 g block-*co*-polymer Pluronic F127 (F127, Sigma-Aldrich) was mixed at 40 °C until the F127 was fully dissolved. 27.5 mL colloidal silica (10−20 nm, SNOWTEX-O, Nissan Chemical) and 11.14 mL of tetraethyl orthosilicate (TEOS, Sigma-Aldrich) were then added to that solution as silica templates, and the solution was stirred for 2 h. Finally, 27.5 g of 20 wt % phenol resin in ethanol was added as the carbon precursor and the solution was stirred for 1 h at 40 °C. The amount of TEOS and colloidal silica was also varied from the above amounts to tune the pore structure of the porous carbon spheres.

Porous Spherical Carbon (PSC). To synthesize the porous spherical carbon (PSC), an aerosol assisted process was employed using the above-described precursor solution. The solution was fed into an aerosol atomizer (model 3076, TSI Inc.) using nitrogen as a carrier gas, as shown in Scheme 1.[28,29] The aerosols passed through a ceramic tube kept at 400 °C to promote evaporation-induced self-assembly and polymerize the phenol resin. Ethanol was periodically added to the precursor solution during this process to keep the viscosity low enough for the atomizer to continue working, since the solution became more viscous as part of it evaporated. As-formed polymer/silica composite particles were collected on filters heated to 80 °C to avoid solvent condensation and were then carbonized by heating to 900 °C for 2 h under argon flow. The resulting carbon/silica composite particles were etched by 8 wt % HF solution (Alfa Aesar) to remove the silica and thus generate more pores. The final carbon particles were then filtered, rinsed several times with deionized water and ethanol, and dried in an oven at 80 °C.

Nonspherical Porous Carbon Particles (ns-PC). The nonspherical porous carbon (ns-PC) was also prepared by a well-developed EISA method.[27] Typically, the same type of precursor solution was used as for PSC. Here, the solution was spread thinly in glass dishes and evaporated under ambient conditions. The phenol resin based silicate solution was polymerized overnight at 100 °C followed by carbonization at 900 °C for 2 h under argon flow. After dissolution of silica by 8 wt % hydrofluoric acid solutions, the porous carbon was ball-milled for 12 h to break it up into submicrometer sized particles.

Porous Spherical Carbon/Sulfur Composites (PSC/S). Sulfur was incorporated into porous carbon by a melt-diffusion and evaporation approach. Typically, 0.091 g of sublimed sulfur was mixed with 0.039 g of porous carbon (70% sulfur in the mixture) in an Ar filled vessel (20 mL) and heated to 155 °C with a rate of 5 °C/min, then kept 155 °C for 8 h. At this temperature, the molten sulfur can penetrate into and coat the pores of the carbon, thanks in part to the high-surface-area-enabled adsorption of sulfur on porous carbon.[16,21] Then, the mixture contained in the vessel was further heated to 300 °C with rate of 5 °C/min and held at this temperature for 5 h to evaporate sulfur on the surface using relatively high vapor pressure of sulfur (8.048 kPa at 300 °C).[30] For the preparation of PSC/S particles with similar sulfur content (ca. 59%), additional evaporation process at 300 °C was carried out for the carbon/sulfur composites (PSC/S) with excessive sulfur content after initial melt-diffusion and evaporation. After the sulfur filling process, the final mass of the carbon/sulfur composite was measured for the calculation of the actual sulfur loading in the composite (Supporting Information Table S1).

(2). Material Characterization. The size and morphology of the synthesized products were characterized using transmission electron microscopy (TEM) and scanning electron microscopy (SEM). TEM images were taken on JEOL-1200 at an accelerating voltage of 80 kV. High-resolution transmission electron microscopy (HR-TEM) images were taken on a field emission microscope JEOL-2010F at an accelerating voltage of 200 kV. Scanning electron microscopy (SEM) and energy-dispersive X-ray spectroscopy (EDS) were conducted with a FEI NanoSEM 630 scanning electron microscope at accelerating voltages of 1.5 kV and 5 kV. The nanocrystalline structure of material was analyzed by X-ray diffraction (XRD) using a Rigaku Dmax-2000 X-ray powder diffractometer with Cu Kα radiation (λ = 1.5418 Å) under operation voltage and current of 40 kV and 30 mA, respectively. The data were collected over a 2θ range between 20 and 50°. For the pore structure analysis, nitrogen sorption isotherms were carried out at 77 K with a Micromeritics ASAP 2020 analyzer (Micromeritics Instrument Corporation, Norcross, GA). Specific surface areas were calculated by the Brunauer−Emmett−Teller (BET) method using the adsorption branch in a relative pressure range from 0.04 to 0.25. The pore size distribution was calculated from the desorption branch of the N_2 isotherm with the Barrett−Joyner−Halenda (BJH) method. The microporosity (micropore surface area) was analyzed by t-plot method.

(3). Electrochemical Measurements. The cathodes for Li/S batteries were prepared by mixing 80 wt % of carbon/sulfur composite, 10 wt % carbon black (Super-P), and 10 wt % polyvinylidene difluoride (PVdF, Sigma-Aldrich) dissolved in 1-methyl-2-pyrrolidinone (NMP, Aldrich) to form a homogeneous slurry. The slurry was then coated onto aluminum foil. Although carbon is present in the composite, we added carbon black to enhance interparticle electronic connectivity of the composite in the slurry. The coated electrodes were dried at 60 °C under vacuum for 12 h and 1.27 cm^2 size discs were cut from the coated electrode to use as cathodes; each cathode had a sulfur loading of approximately 0.5−0.6 mg/cm^2. Electrochemical tests of these electrode materials were performed using CR2016-type coin cells with the porous carbon/sulfur composite cathode and lithium metal foil (99.9%, Aldrich) as the anode. The electrolyte was 1 M bis(trifluoromethane)sulfonimide lithium salt (LiTFSI, Sigma-Aldrich) and 0.1 M lithium nitrate ($LiNO_3$, Sigma-Aldrich) dissolved in a mixture of 1,3-dioxolane (DOL, Sigma-Aldrich) and dimethoxyethane (DME, Sigma-Aldrich) (DOL:DME, 1:1 v/v). A polypropylene membrane (Celgard 2400) was used as a separator film. The cells were assembled in an argon-filled glovebox (MBraun). Cells were cycled in the voltage range 3.0−1.7 V using a BT-2043 Arbin battery testing system. All capacity values were calculated on the basis of sulfur mass. Cyclic voltammetry measurements were carried out on coin cells at a scan rate of 0.1 mV/s between 1.5 and 3.0 V and AC impedance spectroscopy was performed over a frequency range from 1 MHz to 0.01 Hz using a CHI660d electrochemical test station and Solartron electrochemical test station, respectively. All cells were tested at room temperature.

3. RESULTS AND DISCUSSION

Scheme 1 illustrates an aerosol generating apparatus and the synthesis procedure of the PSCs through an aerosol-assisted route (step I) and subsequent carbonization and template dissolution (step II and III). In step I, spherical mesostructured polymer/silica composite particles are prepared using an aerosol-assisted process (Scheme 1A).[25,26] A solution of phenol resin, F127, silicate (TEOS) and silica colloids are used as the feeding precursor; an atomization process using nitrogen as the carrier gas continuously generates aerosol droplets (Scheme 1B-a). The precursor droplets pass through a heating zone and

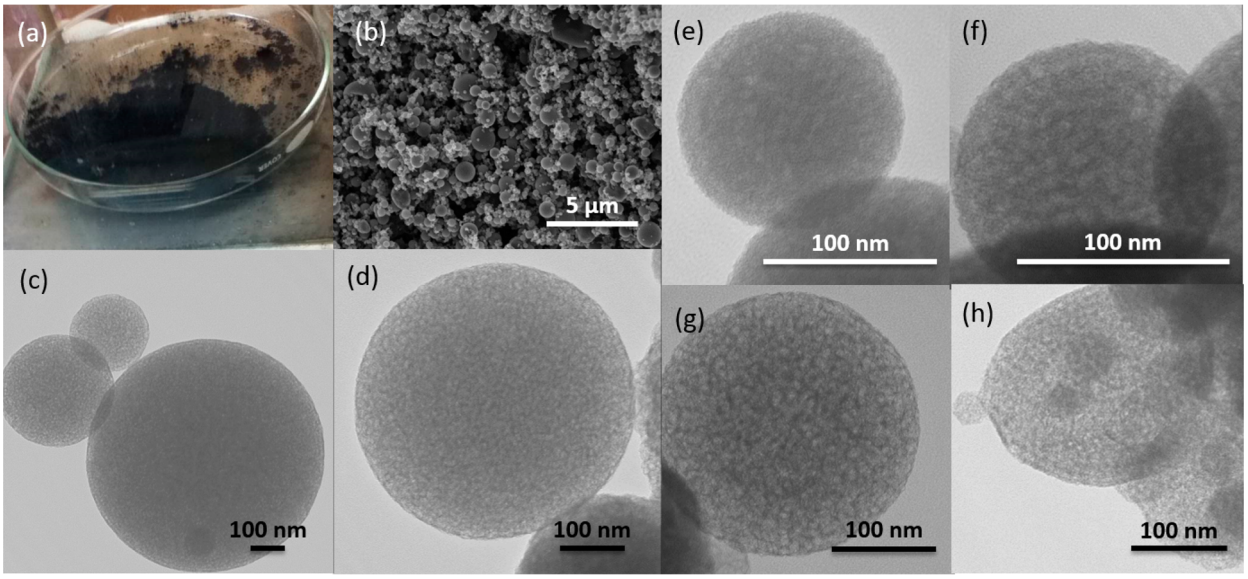

Figure 1. (a) Digital photo image and (b) SEM image of mesoporous carbon sphere (PSC-0); TEM images of porous spherical carbon (PSC): (c and d) PSC-0, (e) PSC-1, (f) PSC-2, (g) PSC-3, and (h) PSC-4.

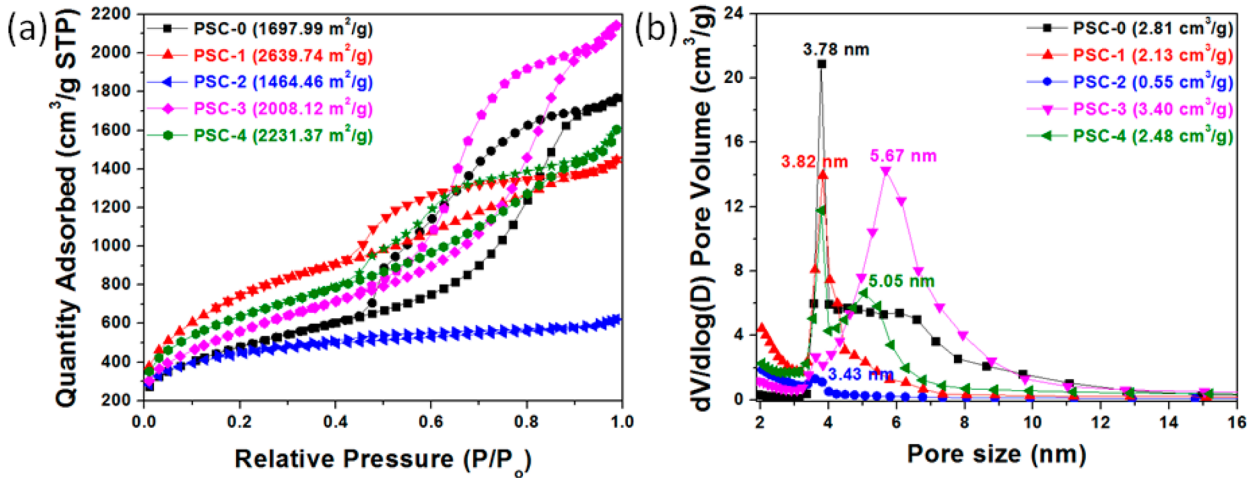

Figure 2. (a) N_2 adsorption/desorption isotherms (inset: BET surface area) and (b) pore size distribution of PSCs (inset: pore volume, marked pore size indicates peak pore size).

Table 1. Pore Structure Parameters of PSCs

	colloidal silica (mL)	F127 (g)	TEOS (mL)	pore vol. (cm^3/g)	BET surface area (m^2/g)	avg. pore size (nm)	sulfur loading (wt %)	theoretical sulfur loading (sulfur)[a]	theoretical sulfur loading (Li_2S)[b]
PSC-0	5.5	1.65	2.228	2.81	1697.99	5.10	60	85.12	76.18
PSC-1	5.5	1.65	6.684	2.13	2639.74	3.69	60	81.51	71.13
PSC-2	5.5	1.65	8.912	0.55	1464.46	3.43	52	53.13	38.83
PSC-3	11	1.65	2.228	3.40	2008.12	5.63	59	87.56	78.47
PSC-4	22	1.65	2.228	2.48	2231.37	4.57	59	83.70	74.76

[a]Theoretical sulfur loading calculated based on the density (2.07 g/cm^3) of sulfur. [b]Theoretical sulfur loading was calculated based on the density (1.66 g/cm^3) of lithium sulfide (Li_2S).

are converted into composite particles (Scheme 1B-b) containing phenol polymer/silicate-F127-silica colloids (step I: a–b). These composites are then carbonized at elevated temperatures (e.g., 900 °C) (step II: b–c) and the remaining silica is dissolved by hydrofluoric acid to obtain hierarchical PSCs (step III: c–d). PSCs are subsequently loaded with sulfur to obtain PSC/S composites and tested as cathode materials for Li/S batteries.

PSCs were characterized by SEM, TEM, and N_2 sorption techniques to determine their morphology, pore structure, and pore size distribution, as displayed in Figures 1 and 2.

Figure 1a shows a photo of a representative PSC (PSC-0; see Table 1 below) synthesized by the aerosol-assisted process. Typically, approximately 2 g of PSC are produced per batch, and the production is continuously operable and scalable by using a larger amount of precursor solution. Figure 1b shows an

dx.doi.org/10.1021/am404508t | ACS Appl. Mater. Interfaces 2014, 6, 7596–7606

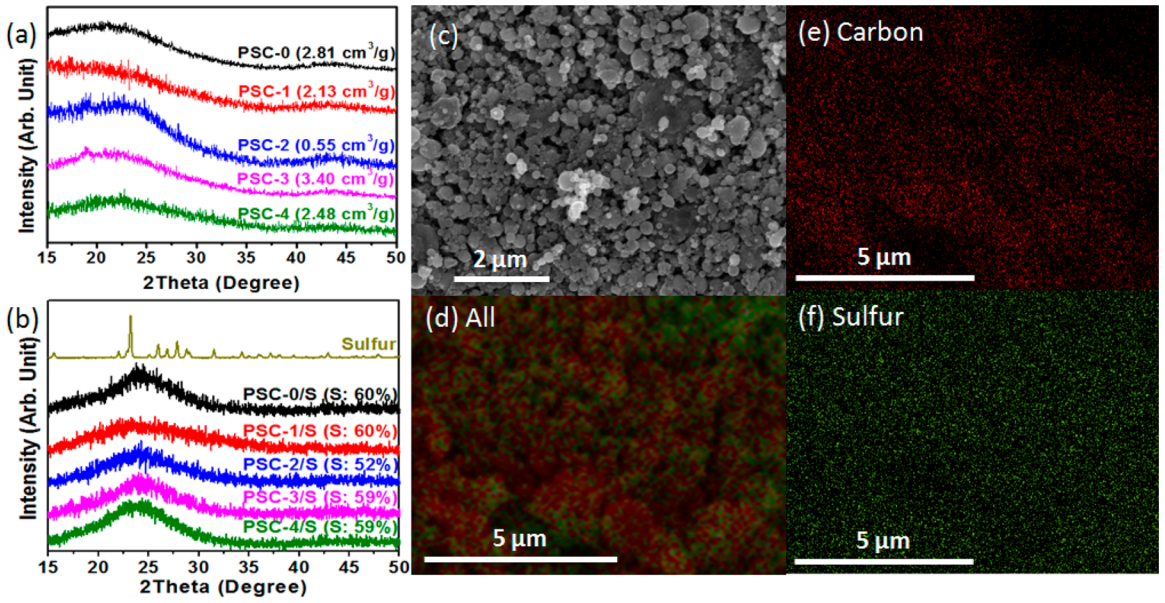

Figure 3. X-ray diffraction of (a) pristine PSCs and (b) elemental sulfur and corresponding sulfur composites of PSCs (PSC/S), where the pore volume (a) and loaded sulfur content (b) are described in parentheses; (c) SEM image of PSC-0/S composites; and elemental mapping of (d) carbon and sulfur, (e) carbon, and (f) sulfur in the PSC-0/S composite.

SEM image of the PSC-0 generated by the aerosol process, showing spherical morphology with a particle size range of approximately 100 nm to 1 μm. Parts c and d of Figure 1 show representative TEM images of PSC-0. Consistent with SEM observation (Figure 1b), the average particle size of the PSC-0 carbon spheres is approximately 300 nm to ~1 μm from TEM images (Figure 1c). The high-magnification TEM image (Figure 1d) shows that the disordered porous structure in PSC-0 is uniform throughout the spheres and the mesopore size is about 5 nm. Other PSCs, prepared using different contents of colloidal silica and TEOS in the precursor solution, also exhibit similar spherical morphology and disordered pore structures (Figure 1e–h).

Figure 2a shows N_2 sorption isotherms and Figure 2b shows BJH pore size distributions of the PSCs. As summarized in Table 1, the BET surface area and total BJH pore volume of the PSCs vary from 1464 m^2/g to 2781 m^2/g and from 0.55 to 3.15 cm^3/g, respectively. As shown in Figure 2a, all PSCs but PSC-2 exhibit a type IV isotherm with adsorption hysteresis, indicating the presence of mesopores.[31] Figure 2b shows the BJH pore size distributions of PSCs, which range from 2 to 16 nm. 5–10 nm mesopores are attributed to the colloidal silica template, while 2–5 nm mesopores are attributed the F127 and TEOS, in accordance with previous literature.[23,27,32] Supporting Information Figure S1 demonstrates regulation of the pore structure (pore volume, pore size, and surface area) of PSCs through controlling the content of TEOS and colloidal silica in the precursor solution. Moderately increasing the amount of TEOS and colloidal silica in the precursor solution increases the surface area (Supporting Information Figure S1c–d) and pore volume (Supporting Information Figure S1a–b) of PSCs, but further increase has the opposite effect. At the same time, significant addition of TEOS (>6 mL) to the precursor reduces average pore size (Supporting Information Figure S1a) and contributes to the formation of microporosity (Supporting Information Figure S1c), whereas addition of more colloidal silica does not significantly affect to the average pore size (Supporting Information Figure S1b) or the microporosity (Supporting Information Figure S 1d).

The PSC/sulfur composites (PSC/S) were characterized by XRD and SEM-EDS elemental mapping (Figure 3). Parts a and b of Figure 3 display XRD patterns for the pristine PSCs and PSC/S composites, respectively. All PSC/S composites except PSC-2/S contained similar amounts of sulfur (ca. 59 wt %). PSC-2/S contained 52 wt % sulfur, likely due to its low pore volume (0.55 cm^3/g); its theoretical sulfur loading (53.13 wt %, Table 1) is correspondingly low. The broad peaks observed around 24° and 44° in the XRD patterns of the PSCs indicate amorphous porous carbons (Figure 3a).[18,24] The XRD patterns of the PSC/S composites (Figure 3b) show similar broad peaks and do not exhibit the characteristic peaks of bulk sulfur. This indicates that sulfur is confined within the mesopores of the PSCs,[16,23] and the sizes of sulfur particles are too small to form crystals. Moreover, as shown in Supporting Information Figure S2, different amounts of sulfur were loaded in PSC-0 to investigate the effect of sulfur loading amount on the structure of PSC/S composite. It was found that PSC-0 (pore volume: 2.81 cm^3/g) with sulfur loading up to 80 wt % still exhibits no reflection peaks of crystalline sulfur in its XRD pattern, indicating that sulfur is constrained to small domains within the pores of the carbon or coated very thinly on the surface of the carbon particles.[16] However, as sulfur content rises above 80 wt %, its XRD pattern acquires peaks belonging to crystalline sulfur, indicating that a portion of sulfur forms larger crystals on the exterior of the particles. Considering the highest sulfur content (theoretical sulfur loading) within the porous spherical carbon can be determined by its pore volume,[24] this result is approximately consistent with the theoretical sulfur loading (85.12%) within pores as calculated from the measured pore volume of PSC-0, as shown in Table 1 and Supporting Information Figure S2.

SEM-EDS elemental mapping was used to characterize morphology and sulfur distribution in the PSC/S composite. PSC-0/S was chosen as an example material for this investigation; Parts c–f of Figure 3 show SEM images and

dx.doi.org/10.1021/am404508t | ACS Appl. Mater. Interfaces 2014, 6, 7596–7606

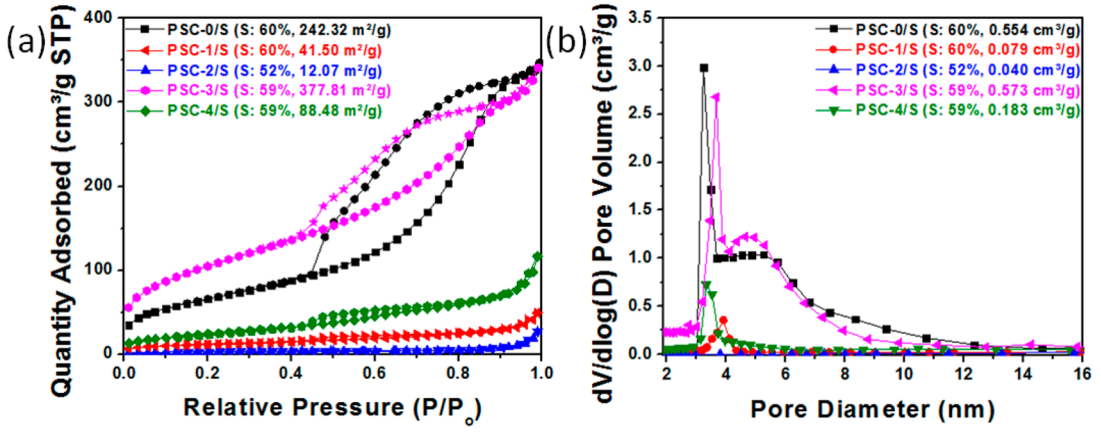

Figure 4. (a) N_2 adsorption/desorption isotherms and (inset: sulfur loading and BET surface area) (b) pore size distribution of PSC/Ss (inset: sulfur loading and pore volume).

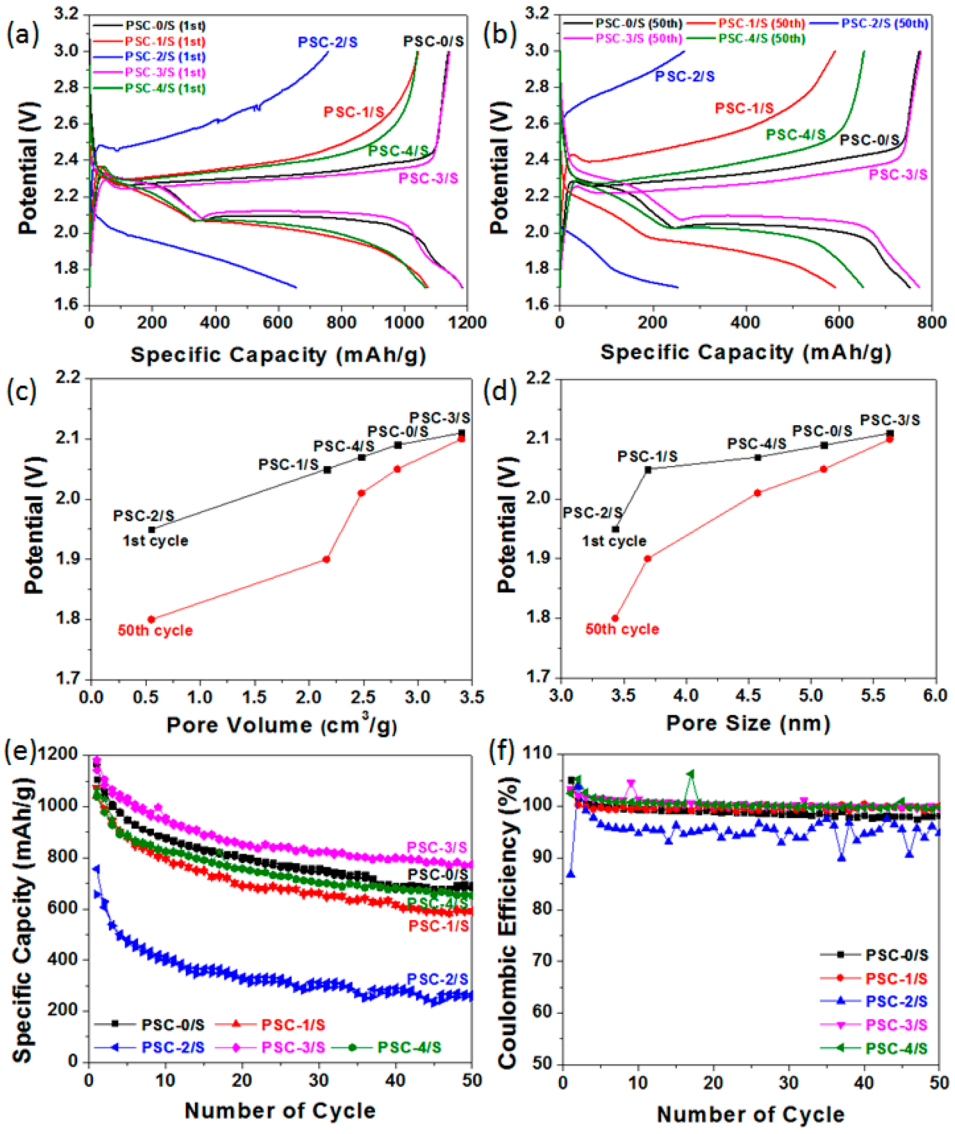

Figure 5. Electrochemical characterization of PSC/S composites (PSC-0/S (S: 60%), PSC-1/S (S: 60%), PSC-2/S (S: 52%), PSC-3/S (S: 59%), and PSC-4/S (S: 59%)) versus lithium at 0.1 C rate. Charge/discharge voltage profiles of (a) the initial cycle and (b) the 50th cycle; potential of plateau region of PSC/S composites at initial and after 50 cycle as related to (c) pore volume and (d) pore size; (e) cycle stability of PSC/S composites; (f) columbic efficiency of PSC/S composites.

dx.doi.org/10.1021/am404508t | ACS Appl. Mater. Interfaces 2014, 6, 7596−7606

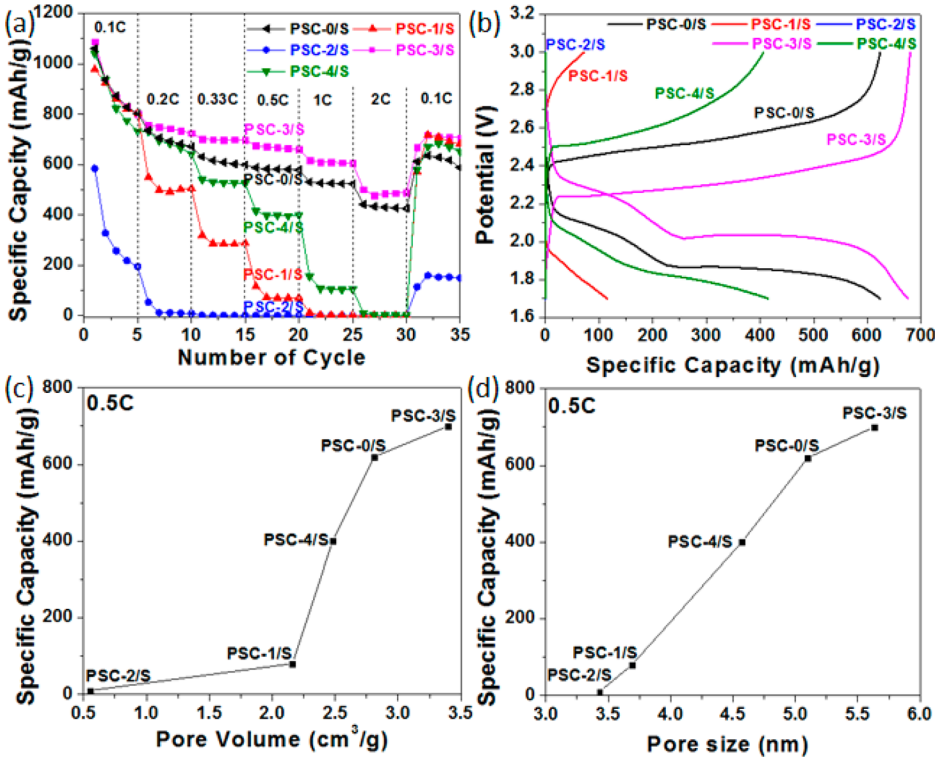

Figure 6. (a) Rate capability of PSC/S composites at different current densities (0.1−2 C), (b) charge/discharge voltage profiles of PSC/S composites at a current density of 0.5 C, (c−d) specific capacity of the PSC/S composites during the rate capability test at 0.5 C correlated with (c) pore volume (cm^3/g) and (d) pore size (nm) of the PSCs.

the EDS elemental maps of PSC-0/S. The PSC-0/S composite has the same spherical morphology as seen in the TEM image of PSC-0 (Figure 1). The elemental maps indicate that sulfur and carbon are distributed uniformly throughout the particles, suggesting that the sulfur is homogeneously embedded in the entire porous matrix of PSC-0.

Parts a and b of Figure 4 show N_2 sorption isotherms and BJH pore size distributions of the PSC/S composites, respectively, demonstrating that the pore structure of the composites (N_2 sorption behavior) is similar to that of the PSCs. The BET surface area and total BJH pore volume of the composites vary from 12.07 m^2/g to 377.81 m^2/g and from 0.040 to 0.549 cm^3/g, respectively, in the order of PSC-3/S > PSC-0/S > PSC-4/S > PSC-1/S > PSC-2/S. There is a significant decrease of pore volume and surface area of PSC/S composites after sulfur loading due to pores being partially or fully filled with sulfur. In addition, even in the presence of enough available pore volume to accommodate sulfur, a larger decrease of surface area was observed in PSCs with smaller presulfur-loading pore size and pore volume.

The electrochemical behavior of the PSC/S composites (PSC-0−4/S) were analyzed as a function of the porosity and pore size of the PSCs, as displayed in Figures 5 and 6.

Parts a and b of Figure 5 compare the first and 50th cycle voltage profiles of the PSC/S composites, for charge/discharge tests conducted at a 0.1 C rate (1 C = 1680 mA/g) between 1.7 and 3.0 V (vs Li/Li^+). The discharge voltage plateaus around 2.3 and 2.0 V correspond to the conversion reaction of elemental sulfur to form Li_2S_8 at 2.3 V, high order lithium polysulfides (Li_2S_x, $4 \leq x < 8$) at 2.3−2.0 V and further reduced form of low order lithium polysulfides and lithium sulfide (Li_2S_x $1 \leq x < 4$) at 2.1 V, respectively.[5,9,24,33−35] The reverse reactions, corresponding to the oxidation of low order polysulfides and high order polysulfides, are indicated by the plateaus in the charge curve.[4,5,9] Parts c and d of Figure 5 show the correlation of the overpotentials of the PSC/S composites with the pore volume and pore size of the PSCs. The overpotentials are expressed indirectly in terms of the average potential of the second (~2.1 V) discharge plateau, as the plateau potential decreases with increasing overpotential. As shown in Figure 5c and d, there is a noticeable trend of decreasing first cycle overpotential with increasing pore volume and pore size. After 50 cycles, the overpotential of the two PSC/S composites with the lowest pore volume and pore size (PSC-2/S and PSC-1/S) is significantly higher than that of the remaining three PSC/S composites, and the trend of decreasing overpotential with increasing pore volume in these three composites is also more pronounced. In addition, although there is no observable trend between the surface areas of PSCs vs polarization (Supporting Information Figure S3a), we found that discharge overpotential significantly decreases as surface area of PSC/S (after sulfur loading) vs polarization increases (Supporting Information Figure S3b), as surface area of the PSC/S composites increases with increasing PSC pore volume. We believe this may be ascribed to different mass transport behavior in the different PSC/S cathodes,[36] since larger pore size and open pore volume should facilitate mass transport of polysulfides inside the pores, decreasing the overpotential.

The initial capacity, cycle stability, and coulombic efficiency of the PSC/S composites at 0.1 C between 1.7 and 3.0 V have also been compared as a function of porosity and surface area of the PSCs (Figure 5e−f and Supporting Information Figure S4). First, as displayed in Figure 5e and Supporting Information Figure S4, the initial capacities of the PSC/S composites

dx.doi.org/10.1021/am404508t | ACS Appl. Mater. Interfaces 2014, 6, 7596−7606

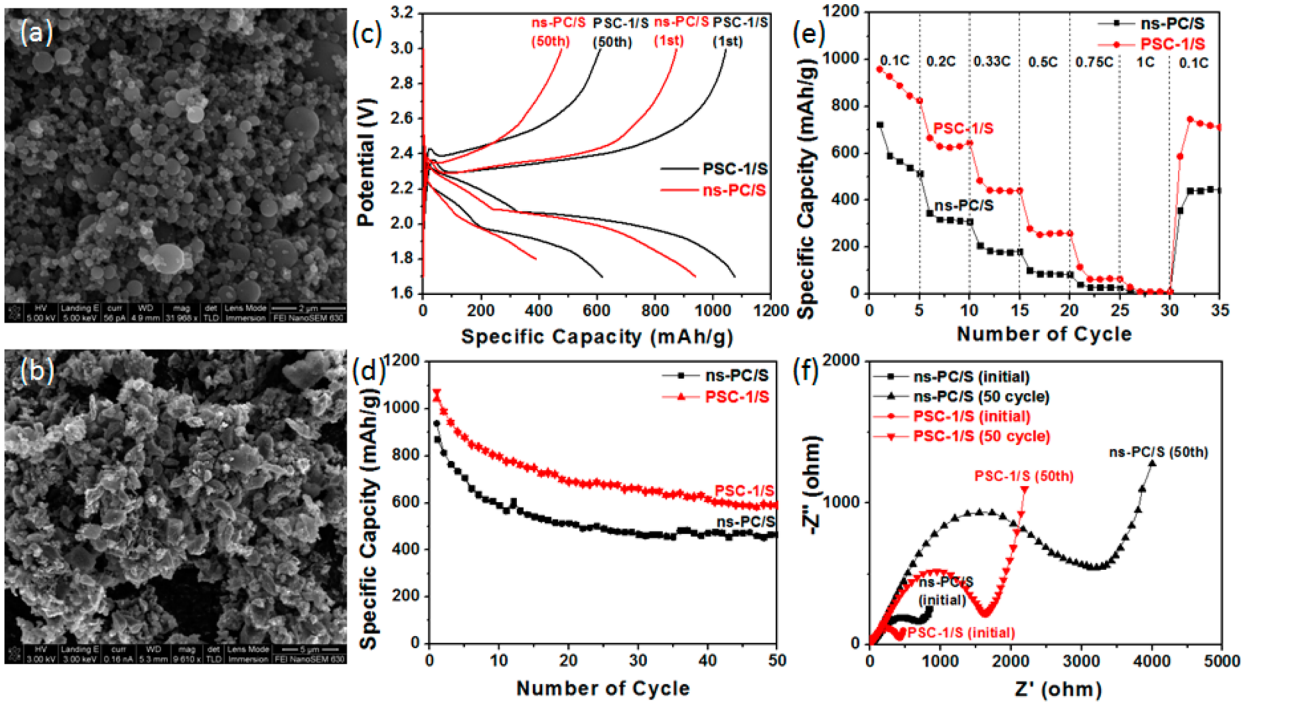

Figure 7. SEM image of (a) PSC-1 and (b) ns-PC, electrochemical performance of PSC-1/S (S: 60%) and ns-PC/S (S: 60%), (c) galvanostatic voltage profile, (d) cycle stability at 0.1C rate, (e) rate capability, and (f) EIS Nyquist plot (1st and 50th cycle).

increase with increasing pore volume and pore size of the PSC. For instance, Supporting Information Figure S4a–b displays that PSC-0/S (2.81 cm^3/g, 5.11 nm) and PSC-3/S (3.40 cm^3/g, 5.63 nm) show the highest initial capacity of 1163 mAh/g and 1181 mAh/g (calculated based on the sulfur), respectively, while PSC-2/S (0.55 cm^3/g, 3.43 nm) exhibits the lowest initial capacity of 656 mAh/g. This is reasonable given that the sulfur loading (52%) is higher than the theoretical sulfur loading (38.83%) calculated based on Li_2S (Table 1).[24] The higher initial capacity can be ascribed to higher sulfur utilization by the PSCs with larger pore volume and pore size; we believe larger pore volume and pore size enable better sulfur infiltration and mass/ion transport.[24,37,44] However, the surface area of the PSCs does not significantly affect their initial capacities (Supporting Information Figure S4c). For instance, despite the similar surface area of PSC-2 (1464 m^2/g) with that of PSC-0 (1698 m^2/g), PSC-2/S exhibits much lower initial capacity (656 mAh/g) than that of PSC-0/S (1163 mAh/g). We also investigated the effect of porosity and surface area on the cycle stability of the PSC/S composites (PSC-0, 1, 3, 4/S) with similar sulfur content (ca. 59%) but did not find noticeable correlation between them; there is no significant difference in the capacity retention of these over cycling. Figure 5f shows that all the PSC/S composites except PSC-2/S exhibit high columbic efficiency (>98%) for all 50 cycles, owing to the $LiNO_3$ additive; $LiNO_3$ is believed to promote the formation of a stable protective film on the lithium anode.[20,24,38−41] The relatively lower columbic efficiency of PSC-2/S suggests that there is a more severe shuttle effect, due to the small pore volume of PSC-2 being unable to fully accommodate the loaded sulfur.[34,42] Overall, the differences in electrochemical performance at 0.1C suggest that lithiation/delithiation can more easily take place in the PSCs with high porosity and pore size, since there is more available space for the lithium polysulfides to transport through the pores and react on the pore surfaces.[18,34,37]

A comparison of the rate performance of all the PSC/S composites and further analyses of their performance as a function of porosity, pore size, and surface area are shown in Figure 6. Figure 6a compares the rate performance of the PSC/S composite cathodes at rates from 0.1C to 2C. At a low rate of 0.1C (168 mA/g), there is no significant difference in specific capacity among the PSCs with relatively large pore volumes (>2 cm^3/g). However, there is bigger difference in specific capacity among the PSCs at higher current density (>0.33C).[37] As the rate increases, the PSC/S composites with larger pore volume and pore size exhibit significantly higher specific capacities than the composites with lower pore volume and pore size. Particularly, PSC-0/S and PSC-3/S exhibit superior performance (441 and 501 mAh/g at 2 C) compared to that of the others (negligible capacity). To gain a better understanding of the electrochemical performance of PSC/S at high rate, we compared the voltage profiles of PSC/S composites at 0.5 C (Figure 6b). PSC-0/S and PSC-3/S show voltage profiles with less polarization and well-defined plateaus, whereas PSC/S composites with smaller porosity show higher polarization and strongly sloped curves.[36] The superior rate capabilities of PSC/S composites with large porosity and pore size further support that large porosity and pore size facilitate efficient mass and ion transport during the charge/discharge process.[36] Parts c and d of Figure 6 further analyze the specific capacities of PSC/S composites at 0.5 C rate (840 mA/g) as a function of pore volume and pore size of PSCs, showing that capacity increases with increasing pore volume and pore size of PSCs. Fast mass transfer is crucial to enabling redox reactions in the cathode during high-rate charge/discharge.[36,43] Larger pore volume and pore size are known to facilitate fast mass transfer,[20,23,24,37] so it is reasonable that the PSC/S composites with larger pore volume and pore size show enhanced rate capability. However,

dx.doi.org/10.1021/am404508t | ACS Appl. Mater. Interfaces 2014, 6, 7596−7606

as shown in Supporting Information Figure S5a, the rate capability of PSC/S does not have a linear relationship with the surface area of the PSCs. Instead, the rate capability of PSC/S is more associated with the surface area of the PSC/S composites (Supporting Information Figure S5b). In addition, it is worthwhile to mention that the current rate capability result is a little different from the report of Zheng et al., who claimed the electrochemical performance could be improved by directly increasing the surface area of the host carbon.[37] We believe the different conclusions originate from the different carbons used in the studies. Zheng et al. compared the electrochemical performance of carbons with various morphologies and properties (Ketjen black, graphene, acetylene black, and hollow carbon nanospheres) without considering the effect of these differences;[37] however, as will be discussed, the morphology can have its own significant effect on electrochemical performance.

As mentioned before, we examined the effect of morphology of porous carbon particles on the electrochemical performance by comparing the PSC-1/S (sulfur content: 60%) cathode against a cathode made with nonspherical porous carbon/sulfur composite (ns-PC/S, sulfur content: 60%) with similar pore volume (PSC-1: 2.13 cm^3/g, ns-PC: 1.96 cm^3/g) and particle size (100 nm to 1 μm). SEM (Figure 7a and b) and TEM images (Supporting Information Figure S6a–b) clearly display the spherical morphology of PSC-1 and irregular morphology of ns-PC. In addition, as shown by the N_2 sorption isotherm and pores size distribution (Supporting Information Figure S6c–d), ns-PC has a mesoporous structure with similar pore volume but different average pore size (PSC-1: 3.7 nm, ns-PC: 7.7 nm). Figure 7c displays charge/discharge voltage profiles for PSC-1/S and ns-PC/S at a 0.1 C rate. The initial capacity of PSC-1/S (1070 mAh/g) is moderately higher than that of ns-PC/S (950 mAh/g). By the 50th cycle, PSC-1/S shows a capacity of 690 mAh/g while the capacity for ns-PC is 465 mAh/g. In addition, PSC-1/S shows less severe polarization than ns-PC/S does, particularly after 50 cycles, even though ns-PC has a bigger average pore size (7.7 nm). Furthermore, as shown in Figure 7d, the PSC-1/S exhibits higher initial capacity than that of ns-PC/S and has good cycle stability up to 50 cycles. Figure 7e compares the rate capability for PSC-1/S and ns-PC/S under different current densities (0.1–1 C). At all current densities, the PSC-1 shows higher capacities than that of ns-PC. In addition, PSC-1/S has a higher tap density (0.820 g/mL) than that of ns-PSC (0.660 g/mL), indicating that PSC-1/S has a higher volumetric energy, as material volumetric capacity is a product of specific capacity and tap density.[23]

The superior electrochemical performance of PSC-1/S to that of ns-PC/S was analyzed by electrochemical impedance spectroscopy (EIS), as shown in Figure 7f. The impedance spectrum of the cell with the PSC-1/S cathode shows a smaller high-frequency semicircle than that of the cell with the ns-PC/S cathode at both the initial and 50th cycle. Since the semicircle in the high frequency region is related to the contact resistance in the bulk electrode,[35,44,45] the smaller semicircle of PSC-1/S indicates better electronic contact between particles, likely originating from the better packing of the spherical particles in the electrode.[23] In addition, the much larger increase in contact resistance of the ns-PC/S cathode compared to that of the PSC-1/S cathode after long cycling indicates faster degradation of the cathode. This may relate to formation of a thicker insulating layer of Li_2S on the surface of the ns-PC/S than on the PSC-1/S. We speculate this can be attributed to the ns-PC/S having more interparticle space that can be filled with Li_2S due to its irregular particle packing. Overall, the better packing enabled by the spherical shape of PSC-1/S provides better electrical connectivity and integration of the active electrode materials, thereby enhancing the electrochemical performance.

4. CONCLUSION

In summary, we have successfully prepared porous spherical carbons with tunable pore structure through a simple and scalable aerosol-assisted process, for use as sulfur hosts for cathodes in lithium/sulfur batteries. The systematic studies on these material revealed that porosity and pore size can efficiently improve electrochemical performance. Particularly, the polarization of the PSC/S composites decreases, especially at high current density (>0.5 C), and the capacity increases with increasing large pore volume and pore size of the PSC due to facilitated mass transport. The effect of morphology on the electrochemical performance of the carbon/sulfur composite was also demonstrated. The spherical carbon/sulfur composite shows superior cycling performance and rate capability to the nonspherical C/S composite. We believe our systematic studies and analyses of the relationship between pore structure/morphology and electrochemical performance can provide good guidance for further development of novel carbon/sulfur composite cathodes for Li/S batteries.

■ ASSOCIATED CONTENT

Supporting Information

Table S1, Figure S1–S6. This material is available free of charge via the Internet at http://pubs.acs.org.

■ AUTHOR INFORMATION

Corresponding Author

*Email: dwang@psu.edu.

Notes

The authors declare no competing financial interest.

■ ACKNOWLEDGMENTS

The authors acknowledge the financial support from the Assistant Secretary for Energy Efficiency and Renewable Energy, Office of Vehicle Technologies of the U.S. Department of Energy, under Contract No. DE-EE0005475.

■ REFERENCES

(1) Xiao, Y.; Zai, J.; Tao, L.; Li, B.; Han, Q.; Yu, C.; Qian, X. $MnFe_2O_4$/Graphene Nanocomposites with Enhanced Performances as Anode Materials for Li-ion Batteries. *Phys. Chem. Chem. Phys.* **2013**, *15*, 3939–3945.

(2) Zai, J.; Wang, K.; Su, Y.; Qian, X.; Chen, J. High Stability and Superior Rate Capability of Three-dimensional Hierarchical SnS_2 Microspheres as Anode Material in Lithium Ion Batteries. *J. Power Sources* **2011**, *196*, 3650–3654.

(3) Tao, L.; Zai, J.; Wang, K.; Zhang, H.; Xu, M.; Shen, J.; Su, Y.; Qian, X. Co_3O_4 Nanorods/graphene Nanosheets Nanocomposites for Lithium Ion Batteries with Improved Reversible Capacity and Cycle Stability. *J. Power Sources* **2012**, *202*, 230–235.

(4) Ji, X.; Nazar, L. F. Advances in Li/S Batteries. *J. Mater. Chem.* **2010**, *20*, 9821–9826.

(5) Manthiram, A.; Fu, Y.; Su, Y.-S. Challenges and Prospects of Lithium/Sulfur Batteries. *Acc. Chem. Res.* **2012**, *46*, 1125–1134.

(6) Chen, R.; Zhao, T.; Lu, J.; Wu, F.; Li, L.; Chen, J.; Tan, G.; Ye, Y.; Amine, K. Graphene-Based Three-Dimensional Hierarchical Sandwich-type Architecture for High-Performance Li/S Batteries. *Nano Lett.* **2013**, *13*, 4642–4649.

(7) Xu, G.; Ding, B.; Nie, P.; Shen, L.; Dou, H.; Zhang, X. Hierarchically Porous Carbon Encapsulating Sulfur as a Superior Cathode Material for High Performance Lithium/Sulfur Batteries. *ACS Appl. Mater. Interfaces* **2014**, *6*, 194−199.
(8) Marmorstein, D.; Yu, T. H.; Striebel, K. A.; McLarnon, F. R.; Hou, J.; Cairns, E. J. Electrochemical Performance of Lithium/Sulfur Cells with Three Different Polymer Electrolytes. *J. Power Sources* **2000**, *89*, 219−226.
(9) Chen, S.; Dai, F.; Gordin, M. L.; Wang, D. Exceptional Electrochemical Performance of Rechargeable Li/S Batteries with a Polysulfide-Containing Electrolyte. *RSC Adv.* **2013**, *3*, 3540−3543.
(10) Yamin, H.; Gorenshtein, A.; Penciner, J.; Sternberg, Y.; Peled, E. Lithium/Sulfur Battery: Oxidation/Reduction Mechanisms of Polysulfides in THF Solutions. *J. Electrochem. Soc.* **1988**, *135*, 1045−1048.
(11) Mikhaylik, Y. V.; Akridge, J. R. Polysulfide Shuttle Study in the Li-S Battery System. *J. Electrochem. Soc.* **2004**, *151*, A1969−A1976.
(12) Cheon, S. E.; Ko, K. S.; Cho, J. H.; Kim, S. W.; Chin, E. Y.; Kim, H. T. Rechargeable Lithium Sulfur Battery I. Structural Change of Sulfur Cathode During Discharge and Charge. *J. Electrochem. Soc.* **2003**, *150*, A800−A805.
(13) Wei Seh, Z.; Li, W.; Chao, J. I.; Zheng, G.; Yang, Y.; McDowell, M. T.; Hsu, P. C.; Cui, Y. Sulphur/TiO_2 Yolk/Shell Nanoarchitecture with Internal Void Space for Long-Cycle Lithium/Sulphur Batteries. *Nature Commun.* **2013**, *4*, 1331−1336.
(14) Wang, J.; Chew, S. Y.; Zhao, Z. W.; Ashraf, S.; Wexler, D.; Chen, J.; Ng, S. H.; Chou, S. L.; Liu, H. K. Sulfur/Mesoporous Carbon Composites in Conjunction with a Novel Ionic Liquid Electrolyte for Lithium Rechargeable Batteries. *Carbon* **2008**, *46*, 229−235.
(15) Liang, C.; Dudney, N. J.; Howe, J. Y. Hierarchically Structured Sulfur/Carbon Nanocomposite Material for High-Energy Lithium Battery. *Chem. Mater.* **2009**, *21*, 4724−4730.
(16) Ji, X.; Lee, K. T.; Nazar, L. F. A Highly Ordered Nanostructured Carbon/Sulphur Cathode for Lithium/Sulphur Batteries. *Nat. Mater.* **2009**, *8*, 500−506.
(17) Lai, C.; Gao, X. P.; Zhang, B.; Yan, T. Y.; Zhou, Z. Triconstituent Co-assembly to Ordered Mesostructured Polymer/Silica and Carbon/Silica Nanocomposites and Large-Pore Mesoporous Carbons with High Surface Areas. *J. Phys. Chem. C* **2009**, *113*, 4712−4716.
(18) Zhang, B.; Qin, X.; Li, G. R.; Gao, X. P. Enhancement of Long Stability of Sulfur Cathode by Encapsulating Sulfur into Micropores of Carbon Spheres. *Energy Environ. Sci.* **2010**, *3*, 1531−1537.
(19) Liang, X.; Wen, Z.; Liu, Y.; Zhang, H.; Huang, L.; Jin, J. Highly Dispersed Sulfur in Ordered Mesoporous Carbon Sphere as a Composite Cathode for Rechargeable Polymer Li/S battery. *J. Power Sources* **2011**, *196*, 3655−3658.
(20) Schuster, J.; He, G.; Mandlmeier, B.; Yim, T.; Lee, K. T.; Bein, T.; Nazar, L. F. Spherical Ordered Mesoporous Carbon Nanoparticles with High Porosity for Lithium-Sulfur Batteries. *Angew. Chem., Int. Ed.* **2012**, *51*, 3591−3595.
(21) Zhang, C.; Bin Wu, H.; Yuan, C.; Guo, Z.; Lou, X. W. Confining Sulfur in Double-Shelled Hollow Carbon Spheres for Lithium/Sulfur Batteries. *Angew. Chem., Int. Ed.* **2012**, *51*, 9592−9595.
(22) Jayaprakash, N.; Shen, J.; Moganty, S. S.; Corona, A.; Archer, L. A. Porous Hollow Carbon@Sulfur Composites for High-Power Lithium/Sulfur Batteries. *Angew. Chem., Int. Ed.* **2011**, *50*, 5904−5908.
(23) Xu, T.; Song, J.; Gordin, M. L.; Sohn, H.; Yu, Z.; Chen, S.; Wang, D. Mesoporous Carbon/Carbon Nanotube/Sulfur Composite Microspheres for High-Areal-Capacity Lithium/Sulfur Battery Cathodes. *ACS Appl. Mater. Interfaces* **2013**, *5*, 11355−11362.
(24) Li, X.; Cao, Y.; Qi, W.; Saraf, L. V.; Xiao, J.; Nie, Z.; Mietek, J.; Zhang, J.-G.; Schwenzer, B.; Liu, J. Optimization of Mesoporous Carbon Structures for Lithium/Sulfur Battery Applications. *J. Mater. Chem.* **2011**, *21*, 16603−16610.
(25) Hampsey, J. E.; Hu, Q.; Rice, L.; Pang, J.; Wu, Z.; Lu, Y. A General Approach towards Hierarchical Porous Carbon Particles. *Chem. Commun.* **2005**, 3606−3608.
(26) Hu, Q.; Kou, R.; Pang, J.; Ward, T. L.; Cai, M.; Yang, Z.; Lu, Y.; Tang, J. Mesoporous Carbon/Silica Nanocomposite through Multicomponent Assembly. *Chem. Commun.* **2007**, 601−603.
(27) Meng, Y.; Gu, D.; Zhang, F.; Shi, Y.; Cheng, L.; Feng, D.; Wu, Z.; Chen, Z.; Wan, Y.; Stein, A.; Zhao, D. A Family of Highly Ordered Mesoporous Polymer Resin and Carbon Structures from Organic-Organic Self-Assembly. *Chem. Mater.* **2006**, *18*, 4447−4464.
(28) Xiao, Q.; Sohn, H.; Chen, Z.; Toso, D.; Mechlenburg, M.; Zhou, Z. H.; Poirier, E.; Dailly, A.; Wang, H.; Wu, Z.; Cai, M.; Lu, Y. Mesoporous Metal and Metal Alloy Particles Synthesized by Aerosol-Assisted Confined Growth of Nanocrystals. *Angew. Chem., Int. Ed.* **2012**, *51*, 10546−10550.
(29) Sohn, H.; Chen, Z.; Jung, Y. S.; Xiao, Q.; Cai, M.; Wang, H.; Lu, Y. Robust Lithium-ion Anodes based on Nanocomposites of Iron Oxide-Carbon-Silicate. *J. Mater. Chem. A* **2013**, *1*, 4539−4545.
(30) Meyer, B. Elemental Sulfur. *Chem. Rev.* **1976**, *76*, 367−388.
(31) Sing, K. S. W.; Everett, D. H.; Haul, R. A. W.; Moscou, L.; Pierotti, R. A.; Rouquerol, J.; Siemieniewska, T. Reporting Physisorption Data for Gas/Solid Systems with Special Reference to the Determination of Surface Area and Porosity. *Pure Appl. Chem.* **1985**, *57*, 603−619.
(32) Liu, R.; Shi, Y.; Wan, Y.; Meng, Y.; Zhang, F.; Gu, D.; Chen, Z.; Tu, B.; Zhao, D. Triconstituent Co-assembly to Ordered Mesostructured Polymer-Silica and Carbon-Silica Nanocomposites and Large-Pore Mesoporous Carbons with High Surface Areas. *J. Am. Chem. Soc.* **2006**, *128*, 11652−11662.
(33) Sun, X.-G.; Wang, X.; Mayes, R. T.; Dai, S. Lithium/Sulfur Batteries Based on Nitrogen-Doped Carbon and an Ionic-liquid Electrolyte. *ChemSusChem* **2012**, *5*, 2079−2085.
(34) Thieme, S.; Bruckner, J.; Bauer, I.; Oschatz, M.; Borchardt, L.; Althues, H.; Kaskel, S. High Capacity Micro- Mesoporous Carbon/Sulfur Nanocomposite Cathodes with Enhanced Cycling Stability Prepared by a Solvent-free Procedure. *J. Mater. Chem. A* **2013**, *1*, 9225−9234.
(35) Deng, Z.; Zhang, Z.; Lai, Y.; Liu, J.; Li, J.; Liu, Y. Electrochemical Impedance Spectroscopy Study of a Lithium/Sulfur Battery: Modeling and Analysis of Capacity Fading. *J. Electrochem. Soc.* **2013**, *160*, A553−558.
(36) Yuan, L.; Qiu, X.; Chen, L.; Zhu, W. New Insight into the Discharge Process of Sulfur Cathode by Electrochemical Impedance Spectroscopy. *J. Power Sources* **2009**, *189*, 127−132.
(37) Zheng, J.; Gu, M.; Wagner, M. J.; Hays, K. A.; Li, X.; Zuo, P.; Wang, C.; Zhang, J.-G.; Liu, J.; Xiao, J. Revisit Carbon/Sulfur Composite for Li-S Batteries. *J. Electrochem. Soc.* **2013**, *160*, A1624−A1628.
(38) Dorfler, S.; Hagen, M.; Althues, H.; Tubke, J.; Kaskel, S.; Hoffmann, M. J. High Capacity Vertical Aligned Carbon Nanotube/Sulfur Composite Cathodes for Lithium/Sulfur Batteries. *Chem. Commun.* **2012**, *48*, 4097−4099.
(39) Zhang, S. S. Role of $LiNO_3$ in Rechargeable Lithium/Sulfur Battery. *Electrochim. Acta* **2012**, *70*, 344−348.
(40) Zhang, S. S. Effect of Discharge Cut off Voltage on Reversibility of Lithium/Sulfur Batteries with $LiNO_3$-Contained Electrolyte. *J. Electrochem. Soc.* **2012**, *159*, A920−923.
(41) Zhang, S. S.; Read, J. A. A New Direction for the Performance Improvement of Rechargeable Lithium/Sulfur Batteries. *J. Power Sources* **2012**, *200*, 77−82.
(42) Su, Y.-S; Fu, Y.; Cochell, T.; Manthiram, A. A Strategic Approach to Recharging Lithium-Sulphur Batteries for Long Cycle Life. *Nature Commun.* **2013**, DOI: 10.1038/ncomms3985.
(43) Park, J.-W.; Ueno, K.; Tachikawa, N.; Dokko, K.; Watanabe, M. Ionic Liquid Electrolytes for Lithium/Sulfur Batteries. *J. Phys. Chem. C* **2013**, *117*, 20531−20541.
(44) Yuan, L.; Yuan, H.; Qiu, X.; Chen, L.; Zhu, W. Improvement of Cycle Property of Sulfur-coated Multi-walled Carbon Nanotubes Composite Cathode for Lithium/Sulfur Batteries. *J. Power Sources* **2009**, *189*, 1141−1146.
(45) Li, K.; Wang, B.; Su, D.; Park, J.; Ahn, H.; Wang, G. Enhance Electrochemical Performance of Lithium Sulfur Battery through a

Solution-based Processing Technique. *J. Power Sources* **2012**, *202*, 389−393.